Structural and functional characterisation of the chlorite dismutase from the nitrite-oxidizing bacterium "Candidatus Nitrospira defluvii": identification of a catalytically import...

ARTICLE *in* JOURNAL OF STRUCTURAL BIOLOGY · DECEMBER 2010

Impact Factor: 3.23 · DOI: 10.1016/j.jsb.2010.06.014 · Source: PubMed

Journal of Structural Biology 172 (2010) 331–342

Contents lists available at ScienceDirect

Journal of Structural Biology

journal homepage: www.elsevier.com/locate/yjsbi

Structural and functional characterisation of the chlorite dismutase from the nitrite-oxidizing bacterium "*Candidatus Nitrospira defluvii*": Identification of a catalytically important amino acid residue

Julius Kostan [a], Björn Sjöblom [a], Frank Maixner [b,1], Georg Mlynek [a], Paul Georg Furtmüller [c], Christian Obinger [c], Michael Wagner [b], Holger Daims [b,*], Kristina Djinović-Carugo [a,d,**]

[a] Department for Structural and Computational Biology, Max F. Perutz Laboratories, University of Vienna, Campus Vienna Biocenter 5, A-1030 Vienna, Austria
[b] Department of Microbial Ecology, Vienna Ecology Centre, University of Vienna, Althanstrasse 14, A-1090 Vienna, Austria
[c] Department of Chemistry, Division of Biochemistry, BOKU – University of Natural Resources and Applied Life Sciences, Muthgasse 18, A-1190 Vienna, Austria
[d] Department of Biochemistry, Faculty of Chemistry and Chemical Technology, University of Ljubljana, Aškerčeva 5, 1000 Ljubljana, Slovenia

ARTICLE INFO

Article history:
Received 19 April 2010
Received in revised form 5 June 2010
Accepted 16 June 2010
Available online 22 June 2010

Keywords:
Chlorite dismutase
Candidatus Nitrospira defluvii
3D-structure
Enzyme kinetics
Structure-based alignment
Site-directed mutagenesis
Catalytic mechanism
Heme proteins
(Per)chlorate bioremediation

ABSTRACT

Chlorite dismutase (Cld) is a unique heme enzyme which transforms chlorite to chloride and molecular oxygen (reaction: $ClO_2^- \rightarrow Cl^- + O_2$). Since bacteria with Cld play significant roles in the bioremediation of industrially contaminated sites and also in wastewater treatment, it is of high interest to understand the molecular mechanism of chlorite detoxification. Here we investigate a highly active Cld from *Candidatus Nitrospira defluvii* (NdCld), a key nitrifier in biological wastewater treatment, using a comprehensive structural, biochemical and bioinformatics approach. We determined the crystal structure of Cld from *Candidatus Nitrospira defluvii* and showed that functional NdCld is a homopentamer possessing a fold found in other Clds and Cld-like enzymes. To investigate the Cld function in more detail, site-directed mutagenesis of a catalytically important residue (Arg173) was performed and two enzyme mutants were structurally and biochemically characterized. Arginine 173 is demonstrated to play a key role in (i) controlling of ligand and substrate access and binding and (ii) in chlorite dismutation reaction. The flexible residue modulates the electrostatic potential and size of the active site entrance and might be involved in keeping transiently formed hypochlorite in place for final molecular oxygen and chloride formation. Furthermore, using a structure-based sequence alignment, we show that the residue corresponding to Arg173 is conserved in all known active forms of Cld and propose it as a marker for Cld activity in yet uncharacterized Cld-like proteins. Finally, our analysis indicates that all Clds and Cld-like enzymes employ a non-covalently bound heme as a cofactor.

1. Introduction

The heme enzyme chlorite dismutase (Cld)[2] was discovered in chlorate- and perchlorate-reducing bacteria (PCRB) (van Ginkel et al., 1996), which are facultative anaerobes using ClO_3^- or ClO_4^- as alternative electron acceptors in absence of oxygen. The reduction of (per)chlorate yields chlorite (ClO_2^-), which is a strong oxidant and has cell-damaging effects (Ueno et al., 2000). At this point Cld comes into play: this enzyme degrades chlorite to Cl^- and O_2 and thus protects PCRB from the accumulation of harmful chlorite. The reaction catalyzed by Cld is not energy-releasing, but is regarded as essential for the survival of PCRB in presence of (per)chlorate. Surprisingly, a highly active Cld was recently identified, characterized, and found to be expressed *in vivo* in the nitrite-oxidizing bacterium "*Candidatus Nitrospira defluvii*" (Maixner et al., 2008). Unlike PCRB, nitrite-oxidizing bacteria (NOB) are aerobic and chemolithoautotrophic organisms that gain energy from the oxidation of nitrite to nitrate. To date, no NOB have been shown to grow by oxidizing nitrite with (per)chlorate as electron acceptor, although this would be energetically possible (Maixner et al., 2008). Furthermore, *Ca. N. defluvii* is a member of the bacterial phylum *Nitrospirae* (Spieck et al., 2006), whereas almost all known PCRB belong to the

* Corresponding author. Fax: +43 1 4277 54389.
** Corresponding author at: Department for Structural and Computational Biology, Max F. Perutz Laboratories, University of Vienna, Campus Vienna Biocenter 5, A-1030 Vienna, Austria. Fax: +43 1 4277 9522.
E-mail addresses: daims@microbial-ecology.net (H. Daims), kristina.djinovic@univie.ac.at (K. Djinović-Carugo).
[1] Present address: Institute for Mummies and the Iceman, EURAC Research, Viale Druso 1, 39100 Bolzano, Italy.
[2] *Abbreviations used:* Cld, chlorite dismutase; PCRB, perchlorate-reducing bacteria; NOB, nitrite-oxidizing bacteria; NdCld, chlorite dismutase of "*Candidatus Nitrospira defluvii*"; SEC, size exclusion chromatography; AoCld, chlorite dismutase of *Azospira oryzae* strain GR-1; DaCld, chlorite dismutase of *Dechloromonas aromatica*; R173K, mutant of NdCld where Arg at position 173 was substituted by Lys; R173A, mutant of NdCld where Arg at position 173 was substituted by Ala; r.m.s.d., root mean square deviation.

1047-8477/$ - see front matter © 2010 Elsevier Inc. All rights reserved.
doi:10.1016/j.jsb.2010.06.014

Proteobacteria. The discovery of an active Cld in *Ca. N. defluvii* (NdCld) raised fundamental questions regarding the evolution of Cld and the biological role of the enzyme in this organism indicating that NOB may possess yet unknown, and fully unexpected, ecophysiological features. Moreover, in the same study (Maixner et al., 2008) all available microbial genomes were screened for genes encoding proteins with homology to known Cld. This search revealed a relatively large superfamily of Cld-like proteins, which extends over a surprising number of bacterial and also archaeal phyla. The known *bona fide* Clds from PCRB and *Ca. N. defluvii* constitute a minor group within this superfamily, whereas the enzymatic activities of the vast majority of the Cld-like proteins are unknown. Merely one Cld-like protein from *Thermus thermophilus* has been characterized both structurally and biochemically, and it was found to have only a weak Cld activity (Ebihara et al., 2005). Cld is of high practical relevance for the bioremediation of the anthropogenic pollutants (per)chlorate and chlorite. These toxic compounds are released into the environment due to industrial processes using (per)chlorate and the application of fertilizers, disinfectants and bleaching agents containing (per)chlorate (Coates and Achenbach, 2004). In addition, Cld is particularly interesting from the biochemical perspective: besides photosystem II, Cld is the only known enzyme whose main function is to catalyze the formation of a covalent O–O bond, which leads to the synthesis of molecular oxygen. However, the catalytic mechanism of chlorite degradation by Cld is not yet completely understood. Significant progress was made recently by Lee et al. (2008), who proposed a mechanism for O–O bond formation by Cld that involves the transfer of one oxygen atom from chlorite to the heme iron, resulting in a compound **I** intermediate, and the subsequent recombination of hypochlorite and compound **I** (Eq. (1)).

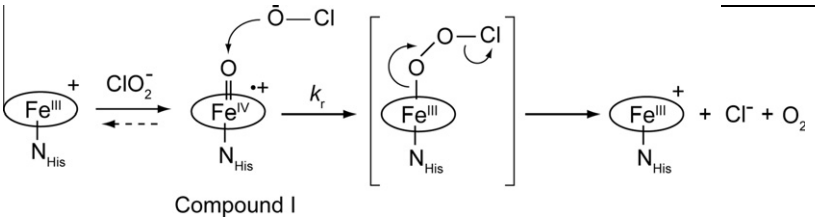

(1)

Further, valuable insight was achieved by analysis of the crystal structure of a highly active Cld, from the betaproteobacterial perchlorate reducer *Azospira oryzae* strain GR-1 (AoCld) (de Geus et al., 2009) and recently by a structure of Cld from *Dechloromonas aromatica* (DaCld) (Goblirsch et al., 2010). Here we report on the structural, bioinformatics and biochemical analyses of the Cld of the nitrite oxidizer *Ca. N. defluvii*. NdCld is the first analyzed, highly active Cld from a non-proteobacterial organism. Based on structural data and theoretical considerations, a particular amino acid residue was previously suspected to play a key role for chlorite degradation (de Geus et al., 2009; Goblirsch et al., 2010), but experimental support for its function was lacking. We addressed this question by studying site-directed mutants of NdCld at the levels of protein structure and enzyme activity. Our results confirm the functional importance of this residue and thus extend current evidence-based knowledge on the catalytic mechanism of Cld. Moreover, we show that this specific residue is conserved in all Clds known to efficiently degrade chlorite and may allow one to predict *in silico* whether yet uncharacterized Cld-like proteins possess a high Cld activity.

2. Materials and methods

2.1. Cloning

The partial gene of NdCld (without the N-terminal signal peptide) was amplified from an enrichment of *Ca. N. defluvii* (Spieck et al., 2006) by PCR and cloned into expression vector pETM11 (EMBL) for the production of a N-terminal His-tagged fusion protein as previously described (Maixner et al., 2008).

2.2. Site-directed mutagenesis

To obtain plasmids for expressing the mutated proteins NdCld R173A or NdCld R173K, where either alanine or lysine was substituted for residue Arg173, mutagenesis was carried out using the QuickChange site-directed mutagenesis kit (Stratagene) with the following primers and their reverse complements: 5′-TATCTGA AGACGGTGAAAGCAAAACTGTATCATTCGAC G-3′, and 5′-CTGAAGA CGGTGAAAAAGAAACTGTATCATTCG-3′, respectively. The plasmid encoding the N-terminal His-tag fusion wild-type NdCld (without the N-terminal signal peptide) was used as template.

2.3. Expression and purification

Native and mutated NdClds were expressed in *Escherichia coli* BL21(DE3) RIL cells (Stratagene) cultivated in heme-enriched (25–50 μM heme *b*) Terrific Broth medium. The N-terminal His-tagged fusion proteins were purified by affinity chromatography using HisTrap HP columns (GE Healthcare). Subsequently, the His-tag was cleaved overnight with TEV protease added at a ratio of 1:100 ($^{w}/_{w}$), and the NdCld was further purified by size exclusion chromatography (SEC) on a HiLoad 26/60 Superdex 200 pg column (GE Healthcare) equilibrated with 20 mM Hepes, 100 mM NaCl, 0.2% glycerol, pH 7.5. In order to obtain protein samples fully loaded with the heme cofactor, purified proteins were mixed with hemin (Fluka) at a molar ratio of 1:2 and incubated for 1 h at room temperature. The last purification step (size exclusion chromatography) served to remove unbound hemin from the mixture. Purified NdClds were concentrated to 15–30 mg/ml and stored at −80 °C until further use.

2.4. Crystallization

Initial attempts to crystallize NdCld, which had been prepared without addition of hemin were performed at 22 °C using the sitting-drop vapor diffusion technique and a nanodrop-dispensing robot (Phoenix™ RE). After 2–3 days 80% of the conditions of PACT Suite crystallization screen (Qiagen) displayed hits. Nevertheless, despite many optimization trials of several selected leads, none

Table 1
Data collection and refinement statistics.

	Data set 1	NdCld:IMD	NdCld:CN	NdCld R173A	NdCld R173 K
Beamline	Home source	ID14–2 (ESRF)	ID14–2 (ESRF)	ID14–2 (ESRF)	ID14–1 (ESRF)
Wavelength (Å)	1.54	0.933	0.933	0.933	0.933
Resolution (Å)	40.7–2.40 (2.45–2.40)[a]	126.0–1.85 (1.9–1.85)	125.0–1.94 (1.99–1.94)	105.4–2.6 (2.67–2.60)	106.0–2.7 (2.77–2.70)
Space group	$P3_221$	$P3_221$	$P3_221$	C2	C2
Unit cell (Å, °)	$a = b = 145.29$, $c = 135.83$	$a = b = 145.67$, $c = 136.44$	$a = b = 145.49$, $c = 136.01$	$a = 139.74$, $b = 113.62$, $c = 120.52$, $\beta = 118.936$	$a = 137.41$, $b = 113.88$, $c = 119.87$, $\beta = 118.020$
Molecules/a.u.	5	5	5	5	5
Unique reflections	126,515 (7108)	268,021 (18,555)	121,048 (17,672)	92,246	80,774 (5070)
Completeness (%)	95.5 (93.3)	97.0 (90.7)	99.2 (99.8)	92.1 (79.9)	91.5 (78.2)
R_{meas}[b]		0.041 (0.351)	0.121 (0.638)	0.171 (0.459)	0.119 (0.474)
R_{pim}[c]	0.0211 (0.2663)				
Multipicity	24.1 (4.36)	5.09 (5.08)	6.4 (6.0)	5.8 (5.9)	4.76 (5.02)
$I/\mathrm{sig}(I)$	14.5 (2.2)	24.4 (5.13)	12.3 (2.1)	8.46 (3.08)	8.67 (3.12)
No. of sites	29				
Phasing power[d]	0.474 (0.150)				
Figure of merit	0.232 (0.090)				
R_{cryst}[e]/R_{free}[f]		0.180/0.210	0.177/0.211	0.212/0.254	0.216/0.258
R.m.s.d. bonds (Å)		0.013	0.012	0.011	0.013
R.m.s.d. angles (°)		1.411	1.322	1.124	1.325

[a] Values in parentheses are for the highest resolution shell. $R_{meas} = \frac{\sum_h \sqrt{\frac{n_h}{n_h-1}} \sum_i^{n_h} |\hat{I}_h - I_{h,i}|}{\sum_h \sum_i^{n_h} I_{h,i}}$ with $\hat{I}_h = \frac{1}{n_h} \sum_i^{n_h} I_{h,i}$.

[b] $R_{mean} = \frac{\sum_h \sqrt{\frac{n_h}{n_h-1}} \sum_i^{n_h} |\hat{I}_h - I_{h,i}|}{\sum_h \sum_i^{n_h} I_{h,i}}$ with $\hat{I} = \frac{1}{n_h} \sum_i^{n_h} I_{h,i}$.

[c] $R_{pim} = \sum_{hkl} \sqrt{\frac{1}{N-1}} \sum_i |I_i(hkl) - \overline{I(hkl)}| / \sum_{hkl} \sum_i I_i(hkl)$ Where I (hkl) is the mean intensity of multiple I_i (hkl) observations of the symmetry-related reflections, N is the redundancy, n_h is the multiplicity, $\hat{I}_h$ is the average intensity and $I_{h,i}$ is the observed intensity.

[d] Anomalous phasing power: $(\Sigma |F_H(\mathrm{imag})|^2 / \Sigma ||\Delta F \pm {}_{PH}(\mathrm{obs})| - |\Delta F \pm {}_{PH}(\mathrm{calc})||^2)^{1/2}$ where $\Delta F \pm {}_{PH}$ is the structure factor difference between Bijvoet pairs and $F_H(\mathrm{imag})$ is the imaginary component of the calculated structure factor contribution by the anomalously scattering atoms.

[e] $R_{cryst} = \Sigma \, |F_o - F_c| / \Sigma \, F_o$.

[f] R_{free} is the cross-validation R_{factor} computed for the test set of reflections (5%) which are omitted in the refinement process.

of them diffracted to better than 4.5 Å resolution. Subsequent crystallization screens with NdClds, which had been fully loaded with heme *b* were performed using the same methodology. The hanging-drop vapor diffusion method was used for the refinement of crystallization conditions of all forms of NdCld using 24-well Linbro plates sealed with siliconized cover slides. Drops (4 µl) containing equivalent amounts of protein and precipitant solutions were mixed and equilibrated against 0.45 ml of reservoir at 22 °C. Wild-type NdCld in complex with imidazole was crystallized in 0.1 M Hepes pH 7.5, 1.4 M sodium/potassium phosphate. Imidazole was found to bind to heme during affinity purification on a HisTrap HP column, and to co-crystallize with NdCld. To obtain cyanide-bound NdCld, the crystals grown under the aforementioned conditions were soaked in 5 mM KCN for 1 h at 22 °C. All soaking steps were performed immediately before flash freezing of crystals in liquid nitrogen. The crystals of the NdCld R173A and R173K mutants were grown from 0.1 M sodium acetate pH 4.6, 1.4 M ammonium phosphate, and 0.1 M citric acid, pH 4.0, 0.4–0.6 M ammonium sulfate, respectively.

2.5. Data collection and processing

Diffraction data from NdCld crystals were collected either in-house on a Bruker Microstar rotating anode at 1.54 Å wavelength X-ray radiation or at various beamlines at ESRF. Diffraction data collected in-house was integrated and scaled using the Proteum2 software suite (Bruker AXS Inc.), while the synchrotron data sets were processed using XDS (Kabsch, 1993). Data collection statistics are summarized in Table 1.

2.6. Phasing

Experimental phases were obtained from a data set (data set 1) collected in-house with 1.54 Å wavelength X-ray radiation using SAD-methodology, exploiting the anomalous signal of iron and sulfur atoms. Heavy atom search, SAD phasing, solvent flattening and auto-building were carried out in autoSHARP (Vonrhein et al., 2007) using SHELXD (Uson and Sheldrick, 1999), SHARP (Vonrhein et al., 2007), SOLOMON (Abrahams et al., 1996) and Arp/wARP (Morris et al., 2003) for the successive steps. All subsequent data sets were phased by molecular replacement using MOLREP (Vagin and Teplyakov, 1997) with the refined NdCld model resulting from data set 1 as a search model.

2.7. Building, refinement and validation of the structure

The structures of native NdCld as well as of the R173A or R173K mutants were refined with Refmac5 (Murshudov et al., 1997). Manual model building was performed in COOT (Emsley and Cowtan, 2004) and final validation of the models was performed with MOLPROBITY (Davis et al., 2004). Data collection and refinement statistics are summarized in Table 1.

2.8. Steady-state kinetics

The stoichiometry of the Cld reaction has been reported to be 1 mol Cl^- and 1 mol O_2 out of 1 mol ClO_2^- (Lee et al., 2008). In this work the release of molecular oxygen was continuously monitored by using a Clark-type electrode (YSI 5331 Oxygen Probe) inserted into a stirred water bath (YSI 5301B) kept at 30 °C. Measurements

were performed in 50 mM phosphate buffer, pH 7.0, and the electrode was equilibrated to 100% air saturation (i.e. 245 μM O_2) by bubbling air to the reaction mixture for at least 15 min. After removal of molecular oxygen from the buffer by bubbling with nitrogen, chlorite was added at different initial concentrations and the reaction was started by addition of 20 and 200 nM solutions of wild-type and mutant NdCld (R173A or R173K), respectively. Molecular oxygen production rates (μM O_2 s^{-1}) were calculated from the initial linear time traces and plotted against chlorite concentrations.

2.9. Transient-state kinetics

For these experiments we used a stopped-flow apparatus (model SX-18MV, Applied Photophysics) equipped for both conventional and sequential measurements. The optical quartz cell with a pathlength of 10 mm had a volume of 20 μl. The fastest time for mixing two solutions and recording the first data point was 1.3 ms. All measurements were performed at 25 °C. Cyanide binding to ferric NdCld was measured in the conventional stopped-flow mode by following the decrease of absorbance at the Soret maximum (410 nm). In a typical experiment, one syringe contained 4 μM NdCld in 50 mM phosphate buffer, pH 7.0, and the second contained at least a 6-fold excess of cyanide in the same buffer. At least six measurements were performed for each ligand concentration. The mean of the pseudo-first-order rate constants, k_{obs}, was used in the calculation of the second-order rate constants obtained from the slope of a plot of k_{obs} *versus* cyanide concentration. In addition cyanide binding to the three heme proteins was also investigated using the diode array detector (Applied Photophysics PD.1) attached to the stopped-flow machine. Normal data sets were analyzed using the Pro-K simulation program (Applied Photophysics), which allowed the synthesis of artificial sets of time-dependent spectra as well as spectral analysis of enzyme intermediates.

2.10. Structural analysis and superposition

Structure comparisons and superpositions were performed by using the SSM server (Protein Structure Comparison Service SSM at EBI) and the program SUPERPOSE of the CCP4-package (CCP4, 1994; Krissinel and Henrick, 2004).

2.11. Phylogenetic analyses of Cld-like proteins

An already existing dataset of aligned amino acid sequences of 174 Clds and Cld-like proteins (Maixner et al., 2008) was manually re-aligned based on the available crystal structures of the following proteins: NdCld from *Ca. N. defluvii*; Cld-like protein from *Geobacillus stearothermophilus* (PDB: 1T0T); Cld-like protein from *Thermoplasma acidophylum* (PDB: 3DTZ); Cld-like protein from *T. thermophilus* (PDB: 1VDH); Cld from *A. oryzae* (PDB: 2VXH). Highly conserved secondary and tertiary structure motifs were used to identify homologous residues in those sequences, which are relatively dissimilar at the primary structure level. Based on the refined alignment and on the 3D-structures, all amino acid residues close to the active site (less than about 4 Å from the heme) were identified, and the conservation of these residues within and between the different phylogenetic lineages of Cld-like proteins was analyzed. Phylogenetic analysis was performed with a subset of 76 of these Cld-like proteins as already described in Maixner et al. (2008). In total 243 alignment columns were used for phylogenetic analysis.

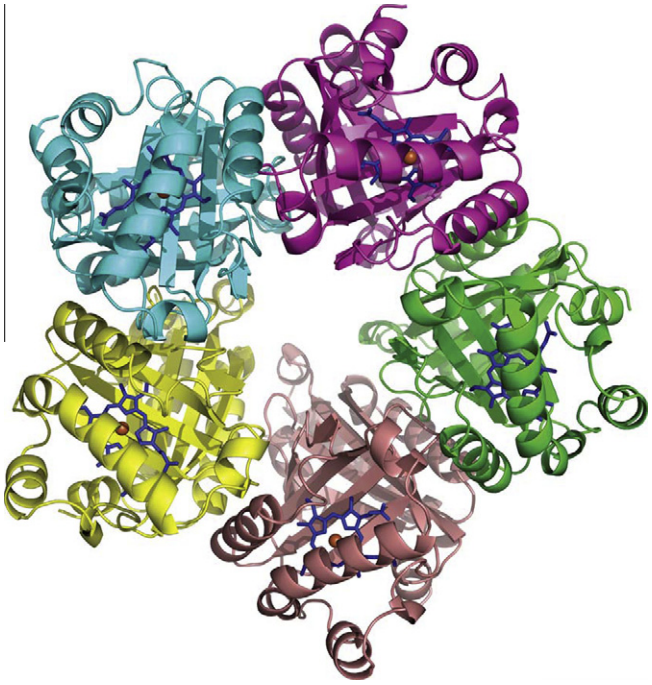

Fig. 1. Crystal structure of Cld from *Ca. N. defluvii*. Ribbon representation of the NdCld structure. Monomers are shown in a unique color. The heme group is shown as a blue sticks model in all monomers. The iron is displayed as a red sphere. View of the pentameric ring-like arrangement of NdCld subumits seen from the proximal site of the heme. All graphic representations were generated using PyMol (DeLano, 2000).

2.12. Miscellaneous

Protein concentrations were determined by using the Lowry assay with bovine serum albumin as standard. Heme type and NdCld:heme *b* stoichiometry were determined by the pyridine hemochrome assay (Berry and Trumpower, 1987), and by using the QuantiChrom™ heme assay kit (BioAssay Systems), respectively.

2.13. Protein data bank accession codes

The atomic coordinates and structure factors (codes 3NN1, 3NN2, 3NN3 and 3NN4) have been deposited in the Protein data Bank, Research Collaboratory for Structural Bioinformatics, Rutgers University, New Brunswick, NJ (http://www.rcsb.org/).

3. Results

3.1. Overall structure

Initial experiments with full length wild-type NdCld had shown that heterologous expression of the complete *cld* gene (including the signal peptide) did not yield a functional enzyme (Maixner et al., 2008). Therefore, we decided to crystallize a version of the enzyme lacking the N-terminal, 26 amino acids long signal peptide necessary for protein export into the periplasmic space. The structure of NdCld in complex with heme *b* was determined using phases from the SAD experiment exploiting Fe and S anomalous signals. Data were collected and crystal structures refined for NdCld in complex with cyanide or imidazole, as well as for two mutant forms of the enzyme, where arginine at position 173 was substituted by either alanine (R173A), or lysine residue (R173K) (for details see Table 1). While wild-type NdCld crystallized in the hexagonal space group $P3_221$, both mutants crystallized in

the monoclinic space group C2 (Table 1). The overall quaternary structure of NdCld was found to be essentially identical through all crystallized proteins, exhibiting five monomers being arranged in a ring-like fashion around a central channel (Fig. 1). This is in good agreement with the result of size exclusion chromatography, giving an approximate molecular weight of 130 kDa for wild-type enzyme and the NdCld mutants. The "donut-shaped" pentamer has an outer diameter of about 80 Å and a height of 70 Å. The central channel is approximately 20 Å in diameter. Thus, the overall structure resembles the architecture previously unveiled for the Cld-like proteins of *T. acidophilum*, *G. stearothermophilus*, *T. thermophilus* HB8 and *D. aromatica* (PDB: 3DTZ, 1T0T, 1VDH; was not available at the time of analyses). The only exception is the structure of the Cld of *A. oryzae* strain GR-1 (PDB: 2VXH), for which a hexameric oligomeric state in the crystal has been reported (de Geus et al., 2009).

3.2. Subunit structure

Each monomer of NdCld is characterized by two topologically equivalent four-stranded antiparallel β-sheets forming a β-barrel, flanked on both sides by six α-helices (Fig. 2A). The order of strands in the β-sheet is 4↑1↓3↑2↓, resembling the topology known as the ferredoxin-like fold, which is seen also in other Cld-like enzymes (de Geus et al., 2009; Ebihara et al., 2005). Two longer helices (α3, α4) span the length of the β-sheet and run approximately parallel to the strands forming a cavity that is closed on one side by two short helices (α2, α5) which are arranged perpendicularly to the β-sheet. The two β-sheets pack together at the angle of about 65°, forming a central flattened β-barrel surrounded on both sides by α-helices. Thus, each NdCld subunit is formed by two structurally similar domains that superimpose with a root mean square deviation (r.m.s.d.) of 2.1 Å over 97 Cα atoms (Fig. 2B). The main differences between the two domains are in the angles that helices α3′ and α4′ form with the β-sheet, resulting in a larger cavity of the C-terminal domain. In addition, in the C-terminal domain the last β-strand β4′ is divided into two parts by a loop (Fig. 2A and B). Comparison of the individual subunits of the pentamer showed that the molecules are almost identical (r.m.s.d. of ~0.4 Å over all Cα atoms). When compared with corresponding subunits of other Cld-like enzymes (PDB: 1T0T, 3DTZ, 1VDH, 2VXH), all subunits superimposed together with a 1.72 Å r.m.s.d. over 180 pairs of structurally equivalent Cα atoms, revealing a high structural conservation of the subunit fold. NdCld showed the highest structural similarity to the AoCld (r.m.s.d. of 0.98 Å over 180 Cα atoms), which had also been crystallized in complex with heme *b* (de Geus et al., 2008). Although the structural comparison with DaCld (Goblirsch et al., 2010) was not possible, on the basis of similarity with AoCld and NdCld we believe that the overall structures will be very similar. The main difference between the structures of Clds with (AoCld, NdCld) and without heme *b* (PDB: 1T0T, 3DTZ, 1VDH), is the orientation of the loop region between β4 and α1' that is partly involved in binding of the prosthetic group and thereby being stabilized in different conformation in apo and holo forms.

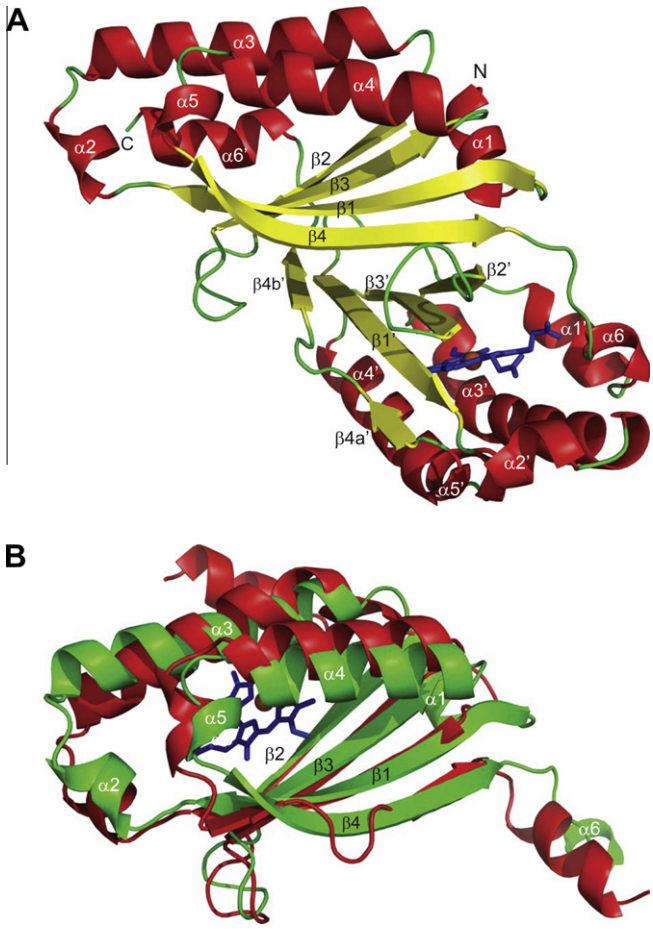

Fig. 2. Structure of a NdCld subunit. (A) The α-helices and β-strands are labeled according to the ferredoxin fold. The NdCld monomer consists of two ferredoxin-like domains, therefore secondary structure elements in the C-terminal domain follow the labeling of the N-terminal domain, with prime mark used as distinguisher. The α-helices and β-strands are shown in red and yellow, respectively. The heme is shown in blue, with iron shown as a red sphere. (B) The N-terminal domain (green) superimposed with the C-terminal domain (red) of the NdCld subunit. Secondary structure elements of N-terminal domain are labeled.

The common interface between neighboring subunits is 1400 Å^2. Since each subunit is in contact with two other molecules, the total area buried in the interfaces is about 23% of the total surface area of a subunit. Each half of a subunit was found to interact with the corresponding half of a neighboring molecule (Fig. 1). The interface consists mainly of residues from helix α4 and strand β4, which interact with residues in the loop between strands β2 and β3 of the neighboring subunit. The compact organization of the NdCld pentamer is dictated by a combination of hydrophobic, ionic and hydrogen-bonding interactions rendering it a stable and functional biological unit.

3.3. Active site

The active site of NdCld is located in the cavity of the C-terminal domain. This cavity, formed by the helices α2′, α3′, α4′ and the β-sheet of the C-terminal domain (Fig. 2A) has a volume of ~1000 Å^3, and was found to accommodate one heme *b* moiety per subunit. Heme *b* is embedded in each cavity within a defined hydrophobic environment, where it is surrounded by Phe114, Lys141, Met157 Ala164, Leu201, Leu205, and Glu210 at the proximal site (Fig. 3A) and residues Leu122, Ile137, Ile139, Val171, Arg173, Phe186, Tyr188, and Phe190 at the distal site (Fig. 3B). The heme iron is coordinated by His160 from the α3′ helix at the proximal side at distances ranging from 2.11 to 2.27 Å (Fig. 3A). Histidine 160 is hydrogen bonded to Glu210, the latter being conserved in Clds with known chlorite dismutation activity. This conserved H-bond increases the imidazolate character of proximal histidine thereby shifting the reduction potential of the heme iron to more negative values (similar to heme peroxidases that have a conserved proximal His-Asp pair). This might be important in stabilization of higher heme oxidation state(s) involved in chlorite dismutation.

Two heme *b* propionate groups form hydrogen bonds to the loop between β4 and α1′, to the α2′ helix, and to the β1′ strand. In detail, one carboxylate group is within hydrogen-bonding

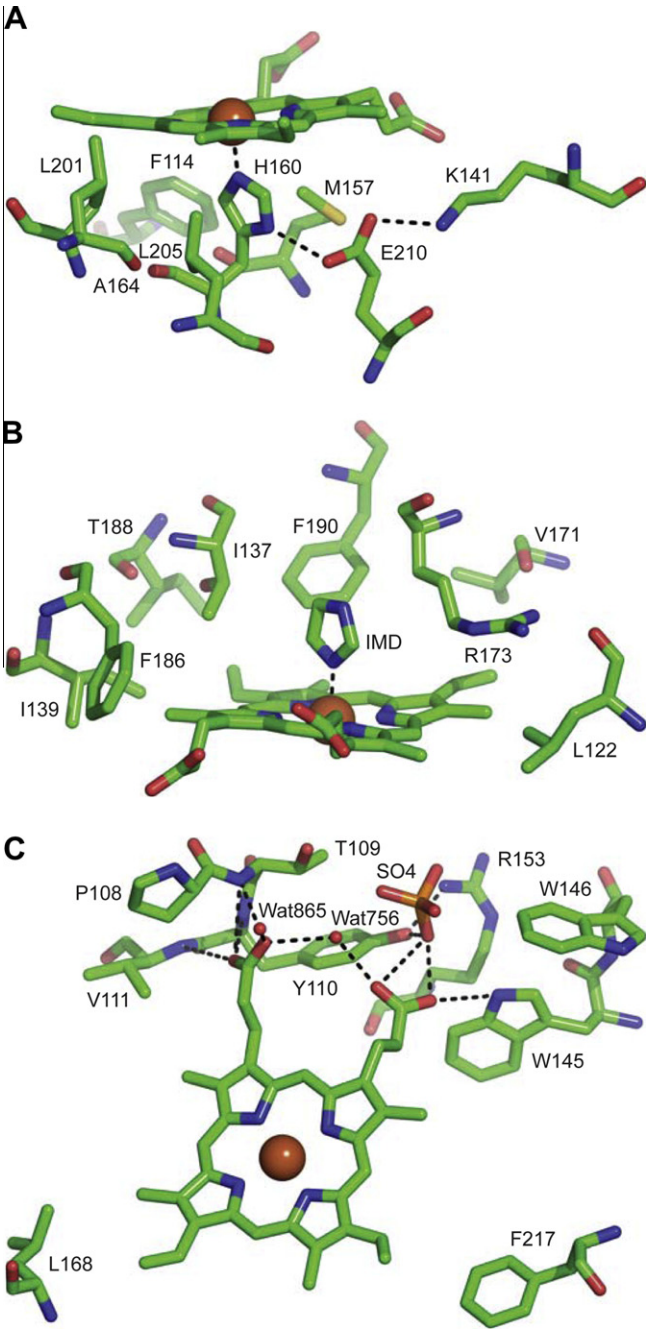

Fig. 3. Heme interactions with NdCld. The figure shows residues interacting with heme in imidazole bound NdCld on its proximal (A), and distal part (B), as well as the interactions between heme propionates and protein (C). The carbon, oxygen, and nitrogen atoms are shown in green, red, and blue, respectively. The sulfur atom of the sulfate anion (*SO4*) is shown in orange. The heme iron and water molecules are shown as red spheres. Hydrogen bonds are drawn as dashed lines. Interactions of heme iron with His160 (*H160*) and imidazole (*IMD*) shown in (A) and (B), respectively, are also indicated by dashed lines.

distances to the main chain amide nitrogen atoms of Thr109, Tyr110 and Val111, while the other carboxylate group interacts with the NE1 atom of Trp145 (Fig. 3C), suggested to act as the electron donor for the reduction of compound **I** to compound **II** (Lee et al., 2008). In the two wild-type NdCld structures reported here, cyanide or imidazole were found to coordinate the iron at the distal heme position (Fig. 4A and B). In each subunit cyanide anion is bound to the heme iron at an average distance of 1.91 ± 0.01 Å and is also within hydrogen-bonding distance to a water molecule and a molecule of glycerol used for cryo protection. Imidazole coordination bond length is 2.18 ± 0.06 Å. In addition, one of the two ethylene glycol molecules was found within hydrogen-bonding distance to the imidazole.

Imidazole was used to elute NdCld from the HisTrap columns and co-purified with the recombinant protein due to high affinity of imidazole to ferric heme. When imidazole-containing crystals were soaked in cyanide, the imidazole was displaced by cyanide at a concentration as low as 5 mM. Both compounds are known to serve as inhibiting ligands of Cld (this study; Hagedoorn et al., 2002; van Ginkel et al., 1996). Hence, the obtained crystal structures represent an inhibited state of Cld at the atomic level.

A close inspection of the distal heme site (Fig. 3B) showed that the only residue able to provide a positive charge, or to shift towards the active site in the presence of an anionic ligand, is Arg173, suggesting that this residue plays an important role in the catalytic reaction of chlorite degradation. In the two NdCld wild-type structures, Arg173 is oriented away from the heme *b* iron and points towards the putative substrate entrance, indicating a possible role of this residue in gating the entrance to the active site. The side-chain of Arg173 is stabilized in this position by hydrogen bonds between the guanidinium and hydroxyl groups of glycerol or ethylene glycol, coming from the cryo-solution, and makes no direct interactions to cyanide or imidazole (Fig. 4A and B). In thiocyanate-bound AoCld no cryoprotectant was found at the corresponding position and the arginine side-chain points towards the heme iron (Supplemental Fig. 1), forming a hydrogen bond to thiocyanate *via* the guanidinium group.

3.4. NdCld mutants

A possible role of Arg (corresponding to position of Arg173 in NdCld) in the ClO_2^- degradation activity of Cld was suggested previously (de Geus et al., 2009; Ebihara et al., 2005), but until now no biochemical or structural evidence has been generated to support this notion. We hence prepared two mutants of NdCld (R173A and R173K) and firstly characterized them at the structural level. As expected, the overall structure of the NdCld mutants remained unchanged compared to wild-type protein (r.m.s.d. of ~0.6 Å over all Cα atoms; all subunits superimposed together). Furthermore, no significant changes in the conformation of the side-chains in the active site of NdCld were observed upon the arginine-to-alanine or arginine-to-lysine substitutions. In the R173K mutant, the Lys173 side-chain adopts a conformation similar to that of Arg183 of AoCld (Supplemental Fig. 1) and forms a hydrogen bond with the sulfate anion found in the active site cavity (Fig. 4D). Additionally, in both mutants a water molecule coordinates the iron at the distal part of heme *b* (at distances of 3.0 and 3.2 Å) (Fig. 4C and D), whereas none of these crystals contained a cryoprotectant molecule close to the active site.

Finally, the most pronounced structural differences between active sites of wild-type and R173K mutant reside in side-chain conformations of Arg173 and Lys173 (Supplemental Fig. 1), suggesting an embedded conformational flexibility for Arg173. This allows it to adopt a conformation similar to Lys173 mutant and to AoCld Arg183 in the active enzyme.

3.5. Steady-state activity

Table 2 summarizes the overall chlorite dismutase activity and apparent bimolecular rate constants of cyanide binding for wild-type NdCld and for the two variants R173A and R173K. Fig. 5A depicts the initial rate of O_2 release followed polarographically as a function of chlorite concentration. An apparent saturation in the initial rate with increasing chlorite concentration is obvious. Data could be best fitted only by a double rectangular hyperbola equation (for better clarity see semi-logarithmic plot in inset to

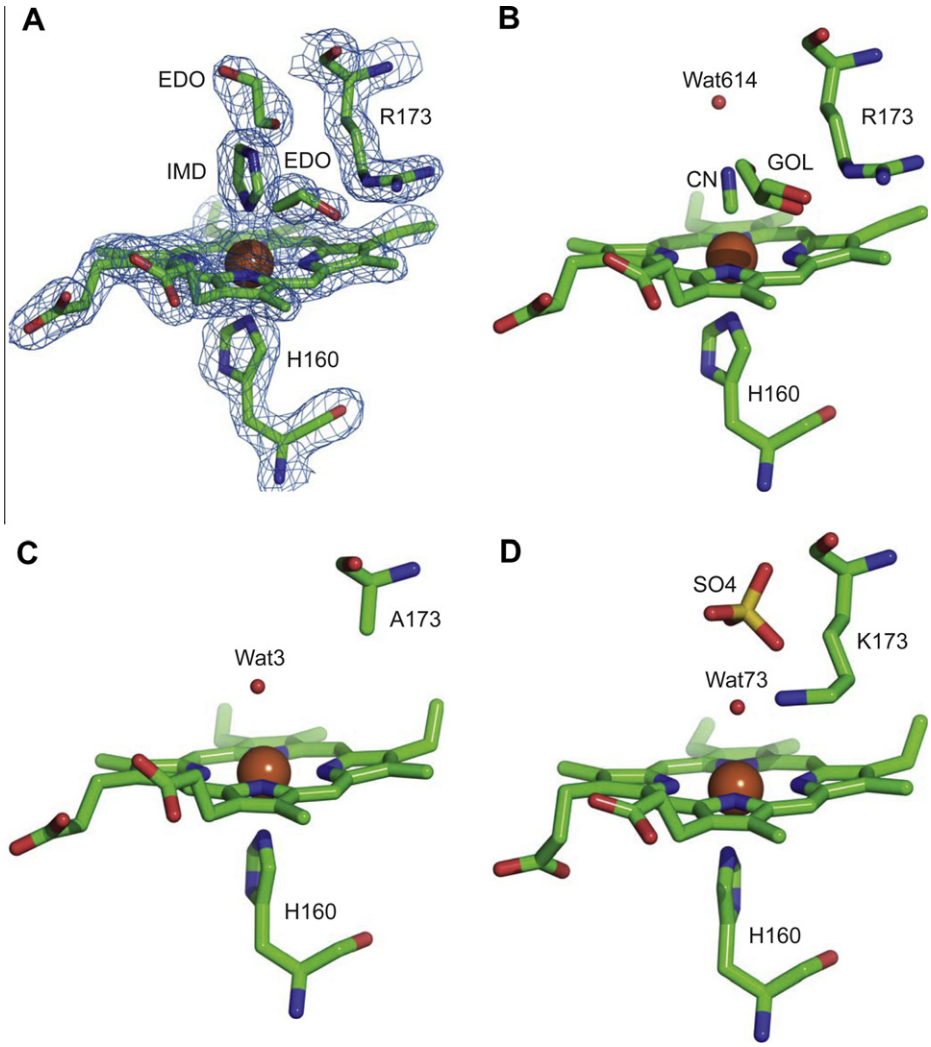

Fig. 4. Active site in wild-type and mutant NdClds. (A) Imidazole (*IMD*) was found to interact with the heme iron at the distal site in the wild-type NdCld. (B) After soaking of wild-type NdCld crystals with KCN, imidazole was effectively replaced by cyanide (*CN*). Water molecules (*Wat*) interact with the heme iron at the distal position in the NdCld R173A (C) and in the NdCld R173K structure (D). Molecules of ethylene glycol (*EDO*), glycerol (*GOL*), or sulfate anions (*SO4*) from cryo-solution (A and B) or reservoir (D) solutions were found in the active site. Atoms are colored as indicated in the legend of Fig. 3. The $|2F_o - F_c|$ electron density map was contoured at the 1.5σ level (A). Note the different orientation of the distal Lys173 in the NdCld R173K mutant (D), compared to Arg173 of the NdCld wild-type shown in (A) and (B).

Table 2
(A) Steady-state kinetic parameters for molecular oxygen evolution of wild-type NdCld and the variants R173A and R173K. (B) Pre-steady-state kinetic parameters for cyanide binding to wild-type NdCld and the variants R173A and R173K.

	Wild-type	R173A	R173K
(A)			
K_M (μM)	58 ± 37	107 ± 54	818 ± 250
k_{cat} (s^{-1})	35	7.1	21
k_{cat}/K_M ($M^{-1}\,s^{-1}$)	6.0×10^5	6.6×10^4	2.5×10^4
(B)			
k_{on} ($M^{-1}\,s^{-1}$)	2.57×10^6	3.43×10^3	1.62×10^3
k_{off} (s^{-1})	9.3	0.50	0.30
K_D (μM)	3.6	145.8	185.2

Fig. 5A). With increasing chlorite concentrations irreversible inactivation of the enzyme occurred as is evident also by inspection of individual time traces depicted in Fig. 5B. Thus, it was important to (i) use only the initial linear phase for rate calculation and to (ii) deduce Michaelis–Menten parameters from a set of chlorite concentrations with $[ClO_2^-] < 1$ mM, which reflect physiological conditions. This also explains why the Michaelis–Menten parameters of NdCld determined here differ from previously reported values (Maixner et al., 2008). In the previous study, the assays were conducted using much higher chlorite concentrations (up to 65 mM), which are unlikely to occur *in situ*. Thus, we regard the values measured here to be more accurate in terms of enzyme activity under natural conditions. For wild-type Cld K_M and k_{cat} were determined to be 58 μM and 35 s^{-1}, resulting in a catalytic efficiency (k_{cat}/K_M) of $6.0 \times 10^5\ M^{-1}\,s^{-1}$. For comparison, the catalytic efficiency and k_{cat} of Cld from *A. oryzae* GR-1 (with the Arg pointing to the heme in the crystal structure) were 11 times and 34 times higher compared to the kinetic parameters of NdCld (van Ginkel et al., 1996).

In principle, both Arg mutants showed the same behaviour as wild-type NdCld, exhibiting kinetics of dioxygen production that could also be fitted best with a double rectangular hyperbola. Compared to the wild-type protein, in both variants the calculated K_M values increased, whereas the k_{cat} values decreased. As a consequence in both mutated enzymes the catalytic efficiency of chlorite dismutation was diminished (Table 2).

3.6. Kinetics of cyanide binding and dissociation

Fig. 5C–E shows the spectral changes of ferric NdCld upon mixing with cyanide. This ligand converts the high-spin ($S = 5/2$) iron

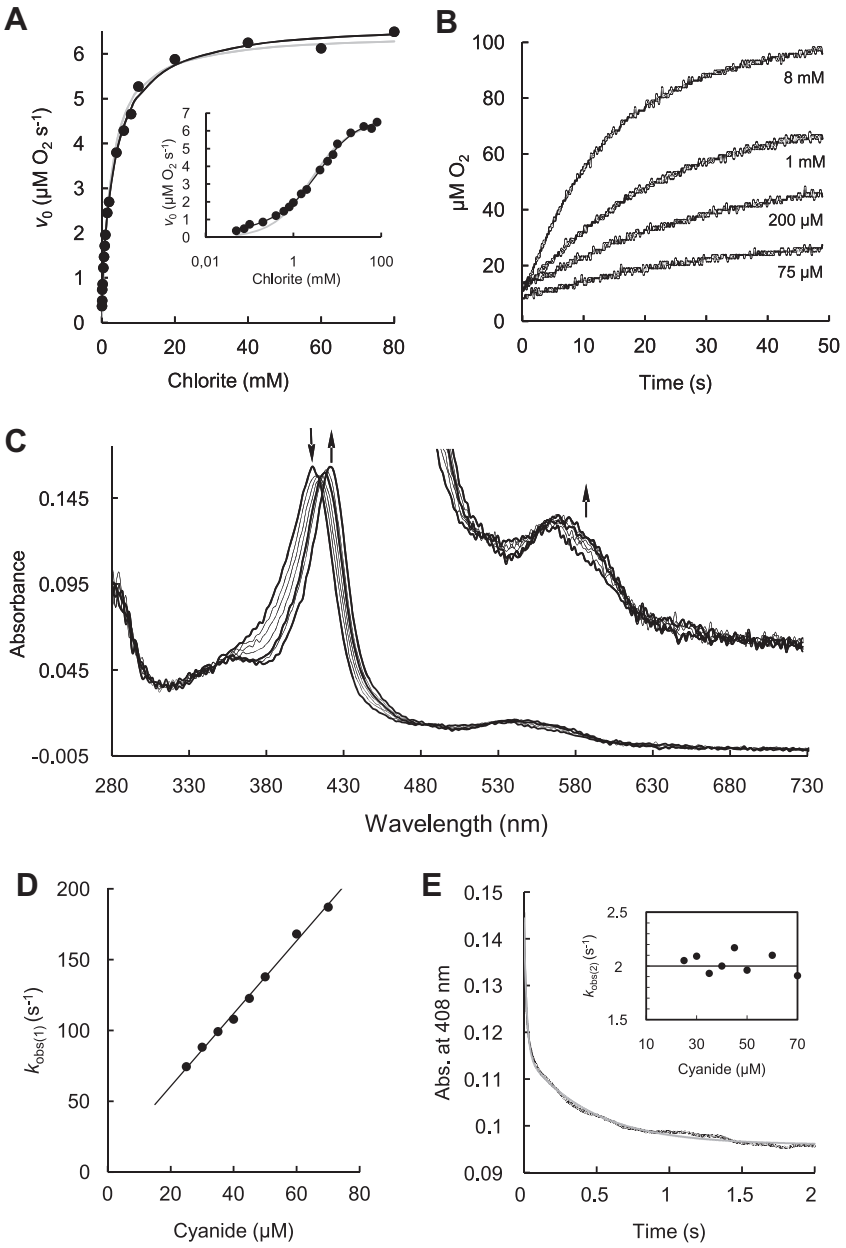

Fig. 5. Monitoring of dioxygen evolution and cyanide binding by wild-type NdCld. (A) Plot of the initial rate (v_0) of molecular oxygen evolution as a function of chlorite concentration. Inset depicts the corresponding semi-logarithmic plot. Points represent averages of three measurements. In addition single- (grey line) and double- (black line) rectangular hyperbolar fits are shown. Conditions: 50 mM phosphate buffer pH 7.0, 20 nM NdCld, 30 °C. (B) Selected time traces with different chlorite concentrations. Conditions as in (A). (C) Spectral transition of the reaction of 2.5 μM Cld with 50 μM cyanide measured in the conventional stopped-flow mode. The first spectrum shows the ferric Cld in its high-spin state. The second spectrum was recorded 1.3 ms after mixing, with subsequent spectra at 3.8, 6.4, 11.5, 40, 109, and 9988 ms showing the formation of the low-spin cyanide complex. Arrows indicate changes of absorbance with time. Conditions: 50 mM phosphate buffer, pH 7, and 25 °C. The spectral transition for the reaction of Cld with cyanide at 408 mn fits to a double-exponential equation. The first exponential term ($k_{obs(1)}$) of the double-exponential equation was dependent on the cyanide concentration whereas the second exponential term ($k_{obs(2)}$) was not (inset). (D) Dependence of $k_{obs(1)}$ values from the cyanide concentration. The association rate constant was calculated from the slope and the dissociation rate constant from the intercept. Final enzyme concentration: 2 μM Cld in 50 mM phosphate buffer, pH 7. (E) Typical time trace at 408 nm with a double-exponential fit (2 μM Cld and 25 μM cyanide). Inset shows the plot of $k_{obs(2)}$ against cyanide concentration.

state to the low-spin ($S = 1/2$) state, thereby shifting the Soret peak from 410 to 422 nm with an intermediate at 418 nm. The first spectral transition from 410 to 418 nm showed a clear isosbestic point at 415 nm, whereas the second spectral transition from 418 to 422 nm did not show any isosbestic point (Fig. 5C). For both mutants cyanide binding was monophasic with a shift of the Soret maximum from 410 to 422 nm and a clear isosbestic point at 418 nm (not shown). By using the stopped-flow apparatus, cyanide binding was followed at 408 nm for all three recombinant proteins. In presence of excess cyanide, pseudo-first-order rate constants, $k_{obs(1)}$ and $k_{obs(2)}$, could be obtained from double-exponential fits for wild-type NdCld (Fig. 5C). In contrast, in both mutants the reactions were monophasic and k_{obs} values could be obtained from single-exponential fits. The apparent second-order rate constant for cyanide binding (k_{on}) was calculated from the slope of the linear plot of $k_{obs(1)}$, or k_{obs} *versus* the cyanide concentration [$k_{obs} = k_{on}[HCN] + k_{off}$] (Fig. 5D). Cyanide binding to wild-type NdCld [$(1.57 \pm 0.07) \times 10^6\ M^{-1}\ s^{-1}$ at 25 °C] was about 460 times faster compared to R173A [$(3.43 \pm 0.07) \times 10^3\ M^{-1}\ s^{-1}$] and 970 times faster than R173K mutant [$(1.62 \pm 0.01) \times 10^3\ M^{-1}\ s^{-1}$]. From the intercept of the linear plots (Fig. 5D) the dissociation rate constants (k_{off}) were obtained, allowing the calculation of the dissociation

constants (K_D) of the cyanide complexes from the k_{off}/k_{on} ratios. The K_D-value for wild-type NdCld is 3.6 μM and increased by factors of 40–50 times for the R173A (146 μM) and R173K (185 μM) mutant, respectively.

3.7. Comparative amino acid sequence analysis of Clds and Cld-like proteins

A multiple sequence alignment of 174 Clds and Cld-like proteins was created by using as template a structure-based sequence alignment of the five crystallized proteins from this superfamily. This alignment allowed us to investigate the conservation of the heme environment in these enzymes from different main microbial lineages of descent (phyla), by analysis of residues located within less than 4 Å distance from the cofactor. The high degree of conservation of heme-binding residues (Supplemental Fig. 2) strongly suggests that all Clds and Cld-like enzymes contain non-covalently bound protoporphyrin IX or heme *b* as cofactor, whereas no analyzed sequence contained the characteristic binding motif (Bowman and Bren, 2008) of covalently bound heme *c* (CXXCH). The proximal heme *b* ligand His160 is highly conserved in the Clds and Cld-like proteins, with the only exception of the respective proteins from *Leptospirillum*, a genus belonging to the *Nitrospirae* phylum. Similarly, functional importance of the Trp145 residue as electron donor is reflected in its full conservation throughout the entire Cld superfamily. The catalytically important residue Arg173 of NdCld, and the homologous residues in other Clds and Cld-like proteins, deserve special attention. At this position, Arg is conserved in the biochemically characterized and highly active Clds of *Ca. N. defluvii* and *A. oryzae* (Supplemental Fig. 2) and in other PCRBs. In contrast, other residues are found in most but not all of the yet uncharacterized Cld-like proteins and in the enzyme from *T. thermophilus*, which has only a very weak Cld activity (Supplemental Fig. 2). This conservation pattern supports the proposed functional role of Arg at this position for efficient chlorite degradation, and is consistent with the low catalytic efficiency of the NdCld mutants R173A and R173K.

4. Discussion

4.1. Functional NdCld is a pentamer

Cld-like enzymes from different sources have been described as tetramers in their native state (Coates et al., 1999; Mehboob et al., 2009; Streit and DuBois, 2008; van Ginkel et al., 1996). In many of these studies classical biochemical approaches such as SEC were used to determine the molecular weight of the protein. In contrast, in most crystal structures of Cld-like enzymes deposited in the PDB database, the proteins were found to exhibit a pentameric organization. The only exception is the structure of AoCld that forms a hexamer in the crystal, although it is pentameric in solution (de Geus et al., 2009). In agreement with other crystal structures we found NdCld to form a pentamer in the crystal, as well as in solution, implying that functional NdCld has a pentameric composition. Thus, since SEC might fail to estimate the real molecular weight, one could speculate that Cld-like enzymes identified as tetramers by SEC actually were pentamers. On the other hand, subunits of Cld-like enzymes may adopt different oligomerization states as was shown for AoCld. It remains to be shown in future experiments whether Cld-like enzymes adopt exclusively a pentameric arrangement in solution.

The active site pocket of NdCld is accessible from the outside of the pentameric ring through two channels one of which is shallower and was in all structures occupied by a sulfate or a phosphate ion. The second opening, observed also in the AoCld structure (de Geus et al., 2009), is deeper with a much higher positive surface potential, suggesting that it could serve both as substrate entry and product exit site (Fig. 6A). In case of R173K mutant the access to the active site through this channel is partially blocked compared to wild-type (Fig. 6B and C), while the R173A mutant exhibits notably smaller reduced positive surface potential (Fig. 6D). The entrance to the active site from the central channel of the holoenzyme, which was reported for the hexameric AoCld (de Geus et al., 2009), was not observed for the pentameric NdCld.

4.2. Structural conservation of Cld fold

Comparisons of known subunit structures of Cld-like enzymes revealed a pronounced structural conservation of the Cld subunit fold (1.72 Å r.m.s.d. over 180 structurally equivalent Cα atoms of all subunits in all available structures), contrasting low average amino acid sequence identity among compared proteins (Supplemental Fig. 2 and Maixner et al., 2008). The main structural differences lay in conformation of the loop region between β4 and α1' which is involved in binding of propionate groups of heme *b*. Subunits of NdCld and AoCld which display the most similar conformation of this region accommodate heme *b* in their active sites, while the prosthetic group is absent in the structures of other Cld-like enzymes (*T. acidophilum*, *G. stearothermophilus* and *T. thermophilus*). Moreover, in the case of the Cld-like protein from *T. thermophilus* HB8, neither the addition of the heme precursor 5-aminolevulinic acid, nor the reconstitution of protein with iron protoporphyrin IX resulted in a protein stoichiometrically loaded with heme (Ebihara et al., 2005). Further research should clarify whether the observed lack of heme in these proteins was an experimental artefact. The heme ligands, which are conserved in almost all of the analyzed sequences including those from *T. acidophilum*, *G. stearothermophilus* and *T. thermophilus* (Supplemental Fig. 2), indicate that the binding of heme cofactor is a common feature of the whole enzyme superfamily.

4.3. Role of Arg173 in chlorite degradation

A role of the guanidinium group of the arginine at position 173 (NdCld numbering) in substrate positioning and activation during chlorite degradation by Cld has been suggested earlier (de Geus et al., 2009). Here, this hypothesis was investigated for the first time in a comprehensive structural, biochemical and bioinformatics approach. Exchange of Arg173 by either Ala or Lys significantly reduced the association rate of cyanide. This low-spin ligand is a useful probe to test the accessibility of the heme cavity and the role of distal residues in its positioning and stabilization of the resulting complex. Similar to hydrogen peroxide in catalases and peroxidases or to chlorite in Cld, cyanide binds in its anionic form and the cyanide complex mimics to some extent higher oxidation states like oxoiron(IV) species (i.e. compound **I** and **II**). The calculated apparent bimolecular k_{on} rates of R173A and R173K were three orders of magnitude lower than that of the wild-type protein. In addition, the dissociation rates were diminished. These data clearly suggest a prominent role of Arg173 in NdCld in low-spin ligand binding to the heme iron.

Both mutants R173A and R173K still exhibited chlorite-degrading activity. Exchange of Arg173 lowered the affinity towards ClO_2^- (Table 2) and the turnover rates of R173A and R173K were diminished. These data suggest that Arg173 is important but not absolutely essential for catalysis. Comparison of wild-type NdCld with the mutants R173K and R173A revealed a remarkable conformational conservation between these structures, clearly demonstrating that Arg173 does not play a key role in the stabilization of the protein structure. Namely, our structural data suggest that Arg173 is flexible and might be involved in the regulation of

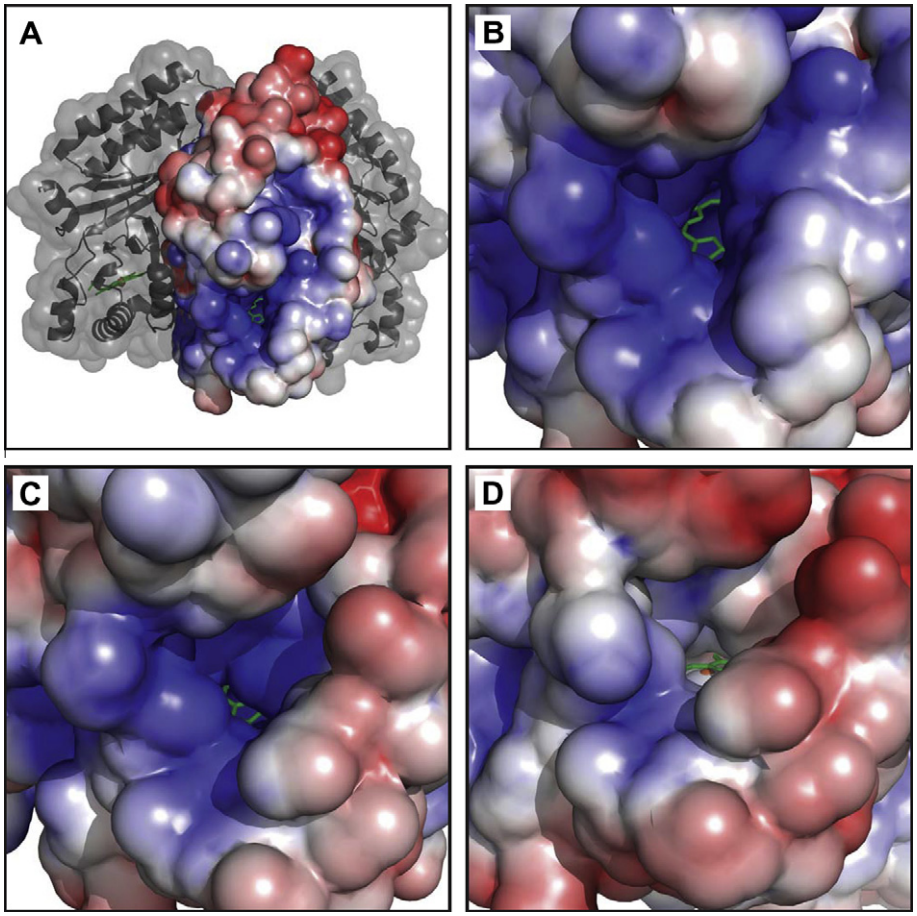

Fig. 6. Molecular surface of the NdCld substrate entrance. (A) The position and accessibility of the heme moiety in NdCld. The solvent accessible surface of one NdCld subunit is colored according to its electrostatic potential (blue for positive, red for negative). The semitransparent surface representations of other NdCld subunits forming the NdCld pentamer are shown in grey, with iron shown as a red sphere. Hemes are presented as green stick models. Detailed view into the active site chamber through the putative substrate entrance and product exit channel in the wild-type NdCld (B), NdCld mutant R173K (C), and NdCld mutant R173A (D). Note the partial blocking of the substrate entrance by the side-chain of Lys173 (C), as well as differences in the entrance surface potential of both mutants (C and D) in comparison to the wild-type NdCld (B).

substrate or ligand uptake and the stabilization of heme complexes or transient reaction intermediates. Such a primary role of Arg173 is in agreement with its properties (charge and shape) and its position at the distal heme side, not far away from the reaction centre and still close to the entrance of the substrate channel. Upon its exchange both the cyanide association rate is reduced and the K_M for chlorite is increased compared to the wild-type protein. Interestingly, the K_M value of R173K was found to be even higher than that of R173A. This suggests a restricted substrate access to the active site in presence of lysine, which is indicated also by the position of lysine *versus* arginine as found in the crystal structures of R173K and wild-type NdCld, respectively (Fig. 4B and D, Supplemental Fig. 1). However, while a significant decrease in k_{cat} was observed for R173A, the k_{cat} of R173K resembled the value of wild-type NdCld. Thus, it seems that in presence of sufficient amount of substrate, lysine may efficiently substitute for arginine, suggesting that a positive charge at this site is important for effective substrate processing. In addition, a positively charged residue will promote the entry of chlorite to the heme cavity through electrostatic attraction. Accordingly, considerable differences in the surface potential at the substrate entrance of the wild-type NdCld and mutant R173A were found (Fig. 6).

Based on the mechanism of the Cld reaction proposed by Lee et al. (2008), compound I (an oxoiron(IV) porphyrin π-cation radical) and ClO^- are formed during the reaction of chlorite with the ferric enzyme. Anionic hypochlorite must remain close to the active site to perform its nucleophilic attack on oxoiron(IV). Since removing the positive charge at position 173 causes a reduction of the overall dismutation rate, it is reasonable to assume that Arg173 helps in addition to stabilize the transient compound **I** – hypochlorite complex. Bleaching of the heme and simultaneous loss of activity upon exposure of Clds to chlorite was observed in several studies and was attributed to the oxidation of the heme (Stenklo et al., 2001; van Ginkel et al., 1996). Consistent with a stabilizing role of the positively charged Arg173 one might also speculate that released hypochlorite contributes to heme bleaching. This fits with the observation that with increasing amounts of chlorite, bleaching of the NdCld heme was faster in R173A compared to both R173K and the wild-type protein (data not shown).

A second anion binding site that could accommodate ClO^- for further transformation has been identified near the active site of AoCld. At this anion binding site, hydrogen carbonate was found to coordinate the strictly conserved residue Lys114 (de Geus et al., 2009). However, as the distance between carbonate and the heme iron in AoCld is 10–12 Å, it appears unlikely that intermediates can be stabilized at this position during the fast chlorite degradation reaction. Thus, although NdCld has a similar anion binding site, we propose that the guanidinium group of Arg173 mainly contributes to keeping ClO^- in place for formation of the O–O bond in the second step of chlorite dismutation.

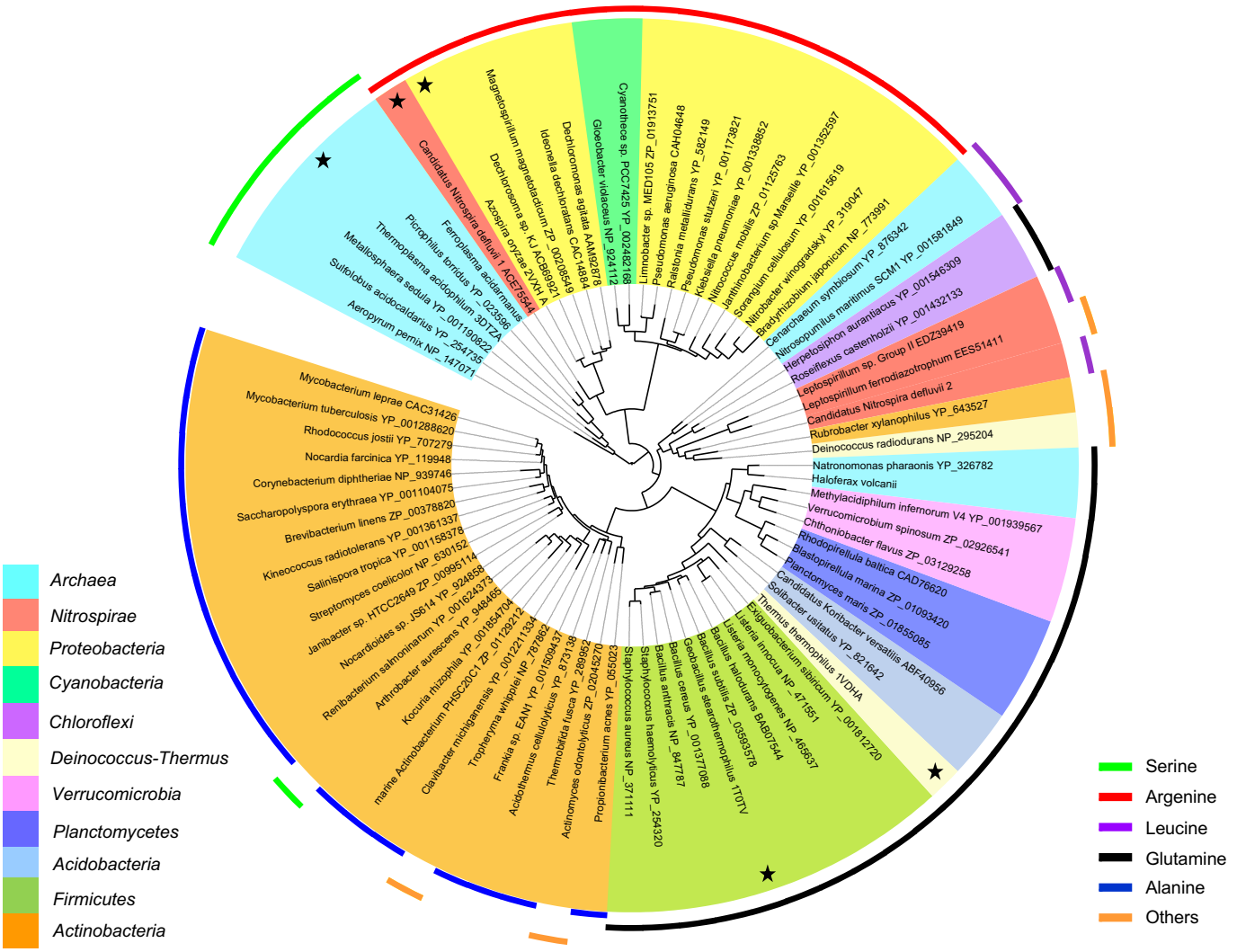

Fig. 7. Maximum likelihood tree based on amino acid sequences of Clds and Cld-like proteins. Sequences marked with an asterix represent crystallized proteins. Colors depict the affiliations of the respective organisms to bacterial and archaeal phyla based on 16S rRNA phylogeny. Colored stripes define the residues at the position, which is homologous to Arg173 of NdCld, in the respective proteins. The circular tree was drawn by using the iTOL online tool (Letunic and Bork, 2007).

4.4. Active site conservation and evolution of Cld

The results of our combined structural and bioinformatics analyses indicate that the second ferredoxin-like domain of Cld subunits has evolved in a protoporphyrin IX or heme *b* binding moiety in all Clds and Cld-like enzymes. The overall high degree of structural conservation allowed us to carry out a phylogenetic analysis, using a structure-based refined alignment, on a set of selected Cld and Cld-like protein sequences. This analysis revealed a similar phylogeny of this enzyme superfamily as discussed in a previous study (Maixner et al., 2008). The reconstructed phylogenetic tree (Fig. 7) shows the wide distribution of Cld-like proteins across the *Bacteria* and *Archaea* with a pronounced grouping of proteins of organisms from the same major phylogenetic lineage (phylum). However, the topology of the protein tree only partly reflects 16S rRNA-based phylogeny. For example, NdCld is closely related to the Clds of proteobacterial PCRB although *Proteobacteria* and *Nitrospirae* are related only at the lowest interphylum level. This observation suggests a functional clustering of Clds and Cld-like proteins in the tree, indicating that closely related enzymes play similar functional roles in the respective organisms. This hypothesis is supported by mapping the homologous amino acid residues at position 173 (NdCld numbering) on the phylogenetic lineages. All validated Clds from known PCRBs and from *Nitrospira*, and yet uncharacterized Cld-like proteins from two bacterial phyla (*Proteobacteria* and *Cyanobacteria*), contain Arg at this position and form a major branch of the enzyme superfamily (Fig. 7). Our experimental results with wild-type NdCld and the mutants R173A and R173K show that a high catalytic efficiency of Cld depends on this Arg residue, which thus may serve as a signature of efficient Clds. On this basis, it is tempting to speculate that the yet uncharacterized Cld-like proteins containing the critical Arg might represent previously overlooked efficient Clds from organisms that were not known to possess this activity. This hypothesis should be verified in future studies, as it could have strong implications for dissecting the composition and structure–function relationships of (per)chlorate-removing microbial consortia. In contrast, in the Cld-like enzyme of *T. thermophilus* the Arg is replaced by Gln, which is also present in a large number of related proteins from other bacterial and archaeal phyla (Fig. 7). As the Cld activity of the protein from *T. thermophilus* is very low (Ebihara et al., 2005), it appears that the Cld-like proteins bearing the Gln residue may share a biological function, which is not chlorite degradation *in vivo*. Likewise, we assume that the Cld-like proteins of most *Actinobacteria*, which host Ala residues, the archaeal enzymes containing Ser, and the forms bearing other residues at position

173 (NdCld numbering) (Fig. 7) represent different functional groups of enzymes. Even though these proteins might still have a detectable but low Cld activity, resembling our NdCld mutants, a primary role of such enzymes in chlorite detoxification appears unlikely. Chlorite is highly reactive and has toxic effects on bacteria already at low concentrations of 10–20 μM (van Wijk et al., 1998). Hence, the high substrate affinity and turnover rates of *bona fide* Clds (containing the Arg residue) should be essential for PCRBs or other organisms, which are exposed to chlorite and are protected by this enzyme.

The presence of both a phylogenetic signal and functional clustering in the protein tree implies that starting from a common ancient motif, structural and functional variants of Cld-like proteins evolved in the different phyla. The presence of similar enzymes in phylogenetically distant organisms can be explained by horizontal gene transfer or, alternatively, by convergent or parallel evolution driven by similar selective pressures. Interestingly, no larger group of organisms (except the PCRB) containing similar Cld-like proteins has obvious ecophysiological traits in common, which could point at possible functions of the respective enzymes. Hence, the biological roles of most proteins in the Cld superfamily, including those which were found in important pathogenic bacteria, remain mysterious, and their experimental clarification will pose an interesting challenge for future research.

5. Conclusions

In this study we provide new data that underline unique structural and functional features of distal Arg173 in Cld. This residue, which is conserved in all sequenced Cld-like enzymes with a confirmed high chlorite dismutation activity, controls and supports ligand and substrate access and binding and keeps transiently formed hypochlorite in place for nucleophilic attack of ferryl oxygen in compound **I**. These findings are in agreement with proposed catalytic mechanism(s) (Lee et al., 2008; Streit and DuBois, 2008). The presence of this Arg residue in yet uncharacterized Cld-like proteins indicates a broader distribution of Clds, and the ability to detoxify chlorite, among microbes than was previously anticipated. Furthermore, based on our structural and bioinformatics analysis we postulate that all Clds and Cld-like enzymes do noncovalently bind protoporphyrin IX or heme *b*.

Acknowledgments

This work was funded by the University Research Focus "Symbiosis research and molecular principles of recognition" of the University of Vienna (Project No. FS573001 "Molecular Interactions between intracellular bacteria and their eukaryotic cells"). We acknowledge the European Synchrotron Radiation Facility for provision of synchrotron radiation facilities and we would like to thank Andrew Mc Carthy, Jens Radzimanowski, Ricardo Leal and Tobias Klar for assistance in using beamlines ID14-1 and ID14-2.

Appendix A. Supplementary data

Supplementary data associated with this article can be found, in the online version, at doi:10.1016/j.jsb.2010.06.014.

References

Abrahams, J.P., Buchanan, S.K., Van Raaij, M.J., Fearnley, I.M., Leslie, A.G., Walker, J.E., 1996. The structure of bovine F1-ATPase complexed with the peptide antibiotic efrapeptin. Proc. Natl. Acad. Sci. USA 93, 9420–9424.

Berry, E.A., Trumpower, B.L., 1987. Simultaneous determination of hemes *a*, *b*, and *c* from pyridine hemochrome spectra. Anal. Biochem. 161, 1–15.

Bowman, S.E., Bren, K.L., 2008. The chemistry and biochemistry of heme *c*: functional bases for covalent attachment. Nat. Prod. Rep. 25, 1118–1130.

CCP4, 1994. The CCP4 suite: programs for protein crystallography. Acta Cryst. D 50, 760–763.

Coates, J.D., Achenbach, L.A., 2004. Microbial perchlorate reduction: rocket-fueled metabolism. Nat. Rev. Microbiol. 2, 569–580.

Coates, J.D., Michaelidou, U., Bruce, R.A., O'Connor, S.M., Crespi, J.N., Achenbach, L.A., 1999. Ubiquity and diversity of dissimilatory (per)chlorate-reducing bacteria. Appl. Environ. Microbiol. 65, 5234–5241.

Davis, I.W., Murray, L.W., Richardson, J.S., Richardson, D.C., 2004. MOLPROBITY: structure validation and all-atom contact analysis for nucleic acids and their complexes. Nucl. Acids Res. 32, W615–W619.

de Geus, D.C., Thomassen, E.A., van der Feltz, C.L., Abrahams, J.P., 2008. Cloning, expression, purification, crystallization and preliminary X-ray diffraction analysis of chlorite dismutase: a detoxifying enzyme producing molecular oxygen. Acta Crystallogr. Sect. F Struct. Biol. Cryst. Commun. 64, 730–732.

de Geus, D.C., Thomassen, E.A., Hagedoorn, P.L., Pannu, N.S., van Duijn, E., Abrahams, J.P., 2009. Crystal structure of chlorite dismutase, a detoxifying enzyme producing molecular oxygen. J. Mol. Biol. 387, 192–206.

DeLano, W.L., 2000. The PyMOL Molecular Graphics System on World Wide Web. <http://www.pymol.org>.

Ebihara, A., Okamoto, A., Kousumi, Y., Yamamoto, H., Masui, R., Ueyama, N., Yokoyama, S., Kuramitsu, S., 2005. Structure-based functional identification of a novel heme-binding protein from *Thermus thermophilus* HB8. J. Struct. Funct. Genomics 6, 21–32.

Emsley, P., Cowtan, K., 2004. Coot: model-building tools for molecular graphics. Acta Crystallogr. D Biol. Crystallogr. 60, 2126–2132.

Goblirsch, B.R., Streit, B.R., Dubois, J.L., Wilmot, C.M., 2010. Structural features promoting dioxygen production by *Dechloromonas aromatica* chlorite dismutase. J. Biol. Inorg. Chem.

Hagedoorn, P.L., De Geus, D.C., Hagen, W.R., 2002. Spectroscopic characterization and ligand-binding properties of chlorite dismutase from the chlorate respiring bacterial strain GR-1. Eur. J. Biochem. 269, 4905–4911.

Kabsch, W., 1993. Automatic processing of rotation diffraction data from crystals of initially unknown symmetry and cell constants. J. Appl. Cryst. 26, 795–800.

Krissinel, E., Henrick, K., 2004. Secondary-structure matching (SSM), a new tool for fast protein structure alignment in 3D. Acta Crystallogr. D Biol. Crystallogr. 60, 2256–2268.

Lee, A.Q., Streit, B.R., Zdilla, M.J., Abu-Omar, M.M., DuBois, J.L., 2008. Mechanism of and exquisite selectivity for O–O bond formation by the heme-dependent chlorite dismutase. Proc. Natl. Acad. Sci. USA 105, 15654–15659.

Letunic, I., Bork, P., 2007. Interactive tree of life (iTOL): an online tool for phylogenetic tree display and annotation. Bioinformatics 23, 127–128.

Maixner, F., Wagner, M., Lucker, S., Pelletier, E., Schmitz-Esser, S., Hace, K., Spieck, E., Konrat, R., Le Paslier, D., Daims, H., 2008. Environmental genomics reveals a functional chlorite dismutase in the nitrite-oxidizing bacterium '*Candidatus Nitrospira defluvii*'. Environ. Microbiol. 10, 3043–3056.

Mehboob, F., Wolterink, A.F., Vermeulen, A.J., Jiang, B., Hagedoorn, P.L., Stams, A.J., Kengen, S.W., 2009. Purification and characterization of a chlorite dismutase from Pseudomonas chloritidismutans. FEMS Microbiol. Lett. 293, 115–121.

Morris, R.J., Perrakis, A., Lamzin, V.S., 2003. ARP/wARP and automatic interpretation of protein electron density maps. Methods Enzymol. 374, 229–244.

Murshudov, G.N., Vagin, A.A., Dodson, E.J., 1997. Refinement of macromolecular structures by the maximum-likelihood method. Acta Crystallogr. D Biol. Crystallogr. 53, 240–255.

Spieck, E., Hartwig, C., McCormack, I., Maixner, F., Wagner, M., Lipski, A., Daims, H., 2006. Selective enrichment and molecular characterization of a previously uncultured Nitrospira-like bacterium from activated sludge. Environ. Microbiol. 8, 405–415.

Stenklo, K., Thorell, H.D., Bergius, H., Aasa, R., Nilsson, T., 2001. Chlorite dismutase from *Ideonella dechloratans*. J. Biol. Inorg. Chem. 6, 601–607.

Streit, B.R., DuBois, J.L., 2008. Chemical and steady-state kinetic analyses of a heterologously expressed heme dependent chlorite dismutase. Biochemistry 47, 5271–5280.

Ueno, H., Oishi, K., Sayato, Y., Nakamuro, K., 2000. Oxidative cell damage in Kat-sod assay of oxyhalides as inorganic disinfection by-products and their occurrence by ozonation. Arch Environ. Contam. Toxicol. 38, 1–6.

Uson, I., Sheldrick, G.M., 1999. Advances in direct methods for protein crystallography. Curr. Opin. Struct. Biol. 9, 643–648.

Vagin, A., Teplyakov, A., 1997. MOLREP: an automated program for molecular replacement. J. Appl. Cryst. 30, 1022–1025.

van Ginkel, C.G., Rikken, G.B., Kroon, A.G., Kengen, S.W., 1996. Purification and characterization of chlorite dismutase: a novel oxygen-generating enzyme. Arch. Microbiol. 166, 321–326.

van Wijk, D.J., Kroon, S.G., Garttener-Arends, I.C., 1998. Toxicity of chlorate and chlorite to selected species of algae, bacteria, and fungi. Ecotoxicol. Environ. Saf 40, 206–211.

Vonrhein, C., Blanc, E., Roversi, P., Bricogne, G., 2007. Automated structure solution with autoSHARP. Methods Mol. Biol. 364, 215–230.